Modulation of photorespiration and nitrogen recycling in Fe-deficient cucumber leaves

Modulation of photorespiration and nitrogen recycling in Fe-deficient cucumber leaves
Fabio c

Highlights

- The effect of Fe deficiency on photorespiration has been little investigated.
- Photorespiration is affected by low Fe availability in cucumber leaves.
- Biochemical investigation revealed changes in peroxisome-enzymes.
- PR modulation involves the induction of N-recycling in Fe-deficient leaf.

Abstract

Low Fe availability affects plant production mainly by impairing the photosynthetic pathway, since Fe plays an essential role in chlorophyll synthesis as well as in the photosynthetic electron transport chain. Under these conditions, plant cells require the activation of protective mechanisms to prevent photo-inhibition. Among these mechanisms, photorespiration (PR) has been relatively little investigated in Fe-deficient plants.

The aim of this work was to investigate the effect of Fe deficiency on photorespiration by performing in vivo analysis in leaves as well as biochemical characterization of some PR-related enzyme activities in a peroxisome-purified fraction from cucumber leaves. Modelling of light response curves at both 21 and 2% pO2 revealed a slowing down of PR under Fe deficiency. The activity of some PR-involving enzymes as well as the contents of glycine and serine were affected under Fe deficiency. Furthermore, nitrate reductase, the glutamine synthetase-glutamate synthase (GS-GOGAT) cycle and hydroxypyruvate dehydrogenase isoform activities were differentially altered under Fe deficiency. The dataset indicates that, in Fe-deficient cucumber leaves, the modulation of PR involves the induction of some PR-related pathways, such as the photorespiratory N recycling and cytosolic photorespiratory bypass processes.

Previous article in issueNext article in issue

Keywords

Fe deficiencyIron metabolismPhotorespirationPeroxisome

1. Introduction

Plant growth depends on the availability of mineral nutrients and, among them, iron (Fe) plays an important role because it is essential in several biological processes (Curie and Briat, 2003; Briat and Lobréaux 1997; Thomine and Vert, 2013; Vigani and Murgia, 2018). Among these, the photosynthetic and the respiratory electron transport chains are strongly affected by Fe deficiency, thereby decreasing the energetic support to the plant cell (Vigani et al., 2019).

Despite Fe-deficient leaves displaying a low photosynthetic rate, they are exposed to excess light energy per chlorophyll molecule, enhancing the risks of photoinhibition and photooxidative damage (Abadía et al., 1999; Andersson and Aro, 2001).

Several reports highlight that plants have different ways to reduce the burden of light to chloroplasts, thereby reducing both photoinhibition events and light-triggered chloroplast damage. These include morpho-anatomical changes, thermal dissipation, the xanthophyll cycle, adjustment of chlorophyll antennae size, the water-water cycle, PSI cyclic electron transport and rapid turnover of the D1 protein of PSII (Andersson and Aro, 2001; Kato et al., 2003).

Chlorophyll fluorescence is a useful tool to study the photosynthetic responses in plant species subjected to Fe deficiency, as revealed by previous studies in sugar beet (Beta vulgaris L.) (Belkhodja et al., 1998), peach (Prunus persica L.) (Molassiotis et al., 2006) and pear (Pyrus communis L.) (Morales et al., 2000a, Morales et al., 2000b). Analysis of chlorophyll fluorescence parameters in pear (Morales et al., 2000a), tomato (Solanum lycopersicum L.) (Donnini et al., 2003) and peach plants (Molassiotis et al., 2006) provided evidence of a general increase in non-photochemical quenching (NPQ) in leaves of Fe-deficient plants. Such findings indicate that there is an activation of photoprotective mechanisms, which in turn cause a reduction in maximum photochemical efficiency (Fv/Fm) and photochemical quenching of PSII (qp) along with a decrease of the actual quantum efficiency (ΦPSII) and the intrinsic efficiency of PSII (Φexc) (Morales et al., 2000b).

In addition to the different mechanisms involved in dissipating the excess of reducing power and energy when CO2 assimilation rate is limited, the photorespiratory cycle operating among chloroplasts, peroxisomes, mitochondria and cytosol, helps in protecting chloroplasts from photoinhibition and prevents plants from excessive accumulation of reactive oxygen species (ROS; Wingler et al., 2000; Sunil et al., 2019). Photorespiration (PR) can also dissipate excess reducing equivalents and energy either directly (using ATP, NAD(P)H and reduced ferredoxin) or indirectly (e.g., via alternative oxidase (AOX) and providing an internal CO2 pool). Several authors have found that PR, which originated as a partner of oxygenic photosynthesis millions of years ago, is strictly linked to many pathways of plant metabolism (Timm et al., 2012, Hasunuma et al., 2010; Araújo et al., 2012; Fernie et al., 2013; Voss et al., 2013).

Photorespiration is, therefore, a complex metabolic process which involves four different cellular compartments. Among these, the impairment of both mitochondria and chloroplasts activities under Fe deficiency conditions has been studied and reviewed in Vigani et al. (2019). However, little information is available about the effect of Fe deficiency on peroxisome. The peroxisome is a small and single-membrane-delimited organelle in almost all eukaryotic cells. Recently, investigations have been carried out on the impact of peroxisome function on photosynthesis by screening over 150 Arabidopsis mutant lines defective in the expression of some genes encoding peroxisomal proteins (Li et al., 2019, Li et al., 2019). The authors demonstrated that impaired PR disturbs the balance of ATP and NADPH, leading to the accumulation of H2O2 that, in turn, activates the cyclic electron flow to produce ATP in order to compensate the imbalance of reducing equivalents. Besides the effect on the photosynthetic process, PR induction impacts on N metabolism. It is well known that carbon flux through chloroplast-peroxisome-mitochondria contributes to the so-called photorespiratory N cycle (Keys et al., 1978) which involves an exchange of amino groups between glycine (Gly) and serine (Ser), and the release of NH4+ from Gly followed by its reincorporation into this amino acid via glutamine (Gln) and glutamate (Glu) (Keys et al., 1978). Despite evidence about the modulation of N metabolism under Fe deficiency which has been already reported (Borlotti et al., 2012; Vigani et al., 2017), the regulation of PR and of the photorespiratory N-cycle in Fe-deficient leaves have still been little studied.

Therefore, the aim of this work was to investigate the effect of Fe deficiency on photorespiration in cucumber leaves by characterizing some peroxisome-related enzyme activities and their biochemical link with N metabolism.

2. Material and methods

2.1. Plant material and growth conditions

Seeds of cucumber (Cucumis sativus L. cv. Marketmore ‘76) were surface-sterilized and sown in Agriperlite, watered with 0.1 mM CaSO4, allowed to germinate in the dark at 26 °C for 3 d, and then transferred to plastic boxes containing a nutrient solution with (+Fe) or without (-Fe) the addition of Fe(III)EDTA. The composition of the nutrient solution was as follows: 2 mM Ca(NO)3, 0.75 mM K2SO4, 0.65 mM MgSO4, 0.5 mM KH2PO4, 10 µM H3BO3, 1 µM MnSO4, 0.5 µM CuSO4, 0.5 µM ZnSO4, 0.05 µM (NH4)Mo7O24 and 0.1 mM Fe(III)- ethylenediaminetetraacetic acid (Fe(III)-EDTA; when added). The pH was adjusted to 6.2 with NaOH. Aerated hydroponic cultures were maintained in a growth chamber with a day:night regime of 16:8 h and a photosynthetic photon flux density (PPFD) of 200 µmol m−2 s−1 photosynthetically active radiation (PAR) at the plant level. The temperature was 18 °C in the dark and 24 °C in the light. After 7 days of treatments, well-expanded leaves of plants were harvested and analyzed.

2.2. Gas exchange measurements

Gas exchange parameters were measured in leaves of plants at the end of the treatments using a portable infrared gas analyzer (LI-6400; Li-Cor, Lincoln, NE, USA). Measurements were performed at increasing light from 0 to 2500 µmol m−2 s−1 PPFD and at a leaf temperature of 25 °C, either with air (21% of O2) or a synthetic air mixture containing <2% O2 where N2 replaced O2. In both the cases, the airflow (300 µmol s−1) was humidified by bubbling it in water of which the temperature was maintained lower than that of the leaf surface. When the synthetic air with <2% O2 was utilized, O2 from the bubbling solution was carefully removed by blowing the same synthetic air mixture for 10 min. Photosynthetic CO2 assimilation (A390), stomatal conductance (gs), and the intercellular CO2 concentration (Ci) were determined using the LI-6400 software. Quantum yield for CO2 uptake was determined as the slope of the linear regression of CO2 assimilation versus light intensity above 100 µmol photons m−2 s−1. The dark respiration Rd, was measured by covering the chamber with a black cloth at an ambient CO2 concentration of 350 µmol mol−1. In most cases the R, values stabilized within 45 min.

The response of the net assimilation rate (A) to intercellular CO2 concentration (A/Ci curve) is measured following the procedure reported in Guidi et al. (2017). The leaf was allowing to equilibrate inside the chamber for 10 min at ~390 µmol mol−1 CO2 concentration and saturating irradiance (~1800 µmol m−2s−1). Once a steady-state was reached, the CO2 concentration was decreased stepwise to 50 µmol CO2 mol−1 air. At the end of the measurements, the CO2 concentration was increased stepwise to 1800 µmol mol−1. Measurements were recorded when values of A, Ci and stomatal conductance did not vary at each step within the sequence. The maximum carboxylation rate at sub-stomata CO2 concentration (Vcmax) was measured by fitting Farquhar's equation (Fanquhar et al., 1980).

2.3. Analysis of chlorophyll fluorescence

Chlorophyll fluorescence measurements were performed with a modulated light fluorimeter (PAM-2000 Walz, Effeltrich, Germany) on leaves of cucumber plants grown under control (+Fe) and Fe deficiency (-Fe) conditions for seven days. The F0 was recorded in a 40 min dark-adapted leaves. The frequency of light pulses was programmed at 600 Hz to determine F0 or 20000 Hz to record the kinetics of induction of fluorescence. The maximum fluorescence yield, Fm, was determined with a saturating pulse of 8000 µmol m−2 s−1 PAR for 800 ms. F0 and Fm were subtracted and divided [(Fm–F0)/Fm] to draw the maximum quantum efficiency of PSII photochemistry Fv/Fm. The current

fluorescence yield (Ft) and the maximum light-adapted fluorescence (Fm') were determined in the presence of an actinic illumination of 400 µmol m−2 s−1, and then the PSII quantum efficiency for photochemistry in light conditions, ΦPSII, was computed as the quotient [(Fm'- Ft)/Fm'] (Genty et al., 1989). The coefficient of photochemical quenching, qP, was calculated as (Fm'-Ft)/(Fm'-F0') according to Schreiber et al. (1986). F0' measurements were carried out in the presence of far-red light (7 µmol m−2s−1) in order to fully oxidize the PSII acceptor side. NPQ was calculated as NPQ=(Fm–Fm')/Fm as reported by Bilger (1990). The apparent electron transport rate (ETR) was determined as 0.5 x ΦPSII x PAR x 0.84, where 0.5 accounted for the excitation of both PSII and PSI, and 0.84 represented the average value for leaf absorbance.

2.4. Isolation of peroxisomes from leaves

Isolation of peroxisomes from cucumber leaves was performed according to Reumann et al. (2007, 2009, 2014) with some modifications. Leaves from control (+Fe) and Fe-deficient (-Fe) plants were harvested 7 d after the start of the treatment and then gently ground in a buffer of high osmolarity [170 mM Tricine-KOH, pH 7.5, 1.0 M sucrose, 1% (w/v) albumin serum bovine (BSA), 2 mM EDTA, 5 mM dithiothreitol (DTT), 10 mM KCl, and 1 mM MgCl2) in the presence of protease inhibitors cocktail (0.1 mM PMSF, 0.2 mM benzamide and 0.2 mM ε-aminocaproic acid) using a mortar and a pestle. The suspension was filtered, and chloroplasts were sedimented at 5000 g (1 min). Approximately 20 mL of supernatant was loaded onto a Percoll density gradient prepared in Tris-EDTA (TE) buffer solution (20 mM Tricine-KOH, pH 7.5 and 1 mM EDTA) supplemented with 0.75 M sucrose and 0.2% (w/v) BSA underlaid by 36% sucrose (w/w) in TE buffer [top to bottom gradient composition: 3 mL of 15% Percoll, 9 mL of 38% Percoll, 2 mL each of a mixture of 38% Percoll, and 36% (w/w) sucrose at a ratio of 2:1 and 1:2, and 3 mL of 36% (w/w) sucrose in TE buffer]. The mixed Percoll-sucrose gradients were centrifuged for 12 min at 13,000×g and then 10–20 min at 27,000×g. Co-sedimentation of peroxisomes along with mitochondria and thylakoid membranes by differential centrifugation prior to isopycnic organelle separation increased irreversibly inter-organellar adhesion and peroxisome contamination. However, chloroplasts, thylakoid membranes, and mitochondria were retained mainly in the 15 and 38% (v/v) Percoll fraction near the top of the gradient, intact leaf peroxisomes crossed the Percoll layer and were recovered at the bottom, visible as a whitish diffuse organelle sediment. The peroxisome fractions at the bottom of the gradient of several Percoll gradients were combined, diluted in 36% (w/w) sucrose in TE buffer, washed several times in TE buffer and finally sedimented by centrifugation (30 min, 39,000×g) supplemented with protease inhibitors, and stored in appropriate aliquots, yielding the leaf peroxisomal fraction LP-P1. The enrichment in leaf peroxisomes was high, as determined by Western Blot analysis using catalase and glyoxylate oxidase as markers. Contaminating chloroplasts and mitochondria were estimated to comprise only 0.1 and 1.7% of the total extract, respectively (Reumann et al., 2007).

2.5. Enzymatic activity assays

A catalase (CAT) activity assay was performed according to the method described by Luck (1965). Leaves from control and Fe-deficient plants 7 d after the start of the treatment were ground in a mortar with the addition of liquid nitrogen, polyvinylpyrrolidone (PVPP) 10% (w/w leaves), and buffer in a ratio 1: 2.5 (w:v) (Buffer composition: Tris-HCl 220 mM-pH 7.4; MgCl2 1 mM; KCl 50 mM; Sucrose 250 mM; DTT 1 mM; PMSF (50 mg mL−1 dimethyl sulfoxide, DMSO). The suspension was filtered and then centrifuged at 12000 g for 30 min at 4 °C. The supernatant was recovered and then dialyzed overnight against diluted extraction buffer (approximately 1:50). Degradation of H2O2,

which reflects the catalytic activity of catalase was monitored by spectrophotometric analysis at 240 nm, 25 °C (εm 240 = 39.4 mM−1 cm−1) using Na-phosphate buffer 65 mM pH 7.2 as assay buffer.

Glycolate oxidase (GOX) activity was measured according to Macheroux et al. (1991) in an enzyme-coupled assay using horseradish peroxidase and o-dianisidine to remove hydrogen peroxide generated during oxidation of glycolate. A typical assay mixture contained µ10 L of horseradish peroxidase (1 mg mL−1), 50 µL of o-dianisidine solution (8 mM, 20% Triton X-100), 10 µL of sodium glycolate (1 M), and 930 µL of 0.1 M potassium phosphate buffer, pH 8.3. The reaction was started by adding 10 µL of the GOX sample. Formation of the o-dianisidine radical cation, which reflects the catalytic activity of glycolate oxidase, was monitored by spectrophotometric analysis at 440 nm and at 25 °C (εm 440 = 11,600 M−1 cm-l).

The hydroxypyruvate reductase (HPR) activity assay was measured as described previously by Schwitzguebel and Siegenthaler (1984) in a reaction medium containing 50 mM phosphate buffer (pH 6.2); 0.025% (v/v) TritonX-100; 1 mM KCN 0.2 mM NADH. The addition of 2 mM hydroxy-pyruvate started the reaction, and the oxidation of NADH was followed at 340 nm (εm 340 = 6.22 M-1 cm-l).

For the superoxide dismutase (SOD) activity assay, leaf samples of control and Fe-deficient plants 7 d after the start of the treatment were ground in liquid N2 with 10% (w/w) polyvinylpolypyrrolidone (PVPP) and homogenized in a medium containing: 50 mM K-phosphate buffer (pH 7.00), 1 mM EDTA, 0.05% (v/v) Triton X-100, 1 mM dithiothreitol (DTT), 1 mM Na-ascorbate and 0.50 mM phenylmethylsulphonyl fluoride (PMSF). After centrifugation at 12,000 g for 30 min at 4 °C, the supernatant was collected and dialysed overnight at 4 °C against 1:50 (v/v) diluted buffer. Superoxide dismutase activity was assayed according to the method of Scebba et al. (2003) at 560 nm, based on the enzyme's ability to inhibit the photoreduction of nitrobluetetrazolium (NBT). One enzyme unit was defined as the amount of enzyme inhibiting 50% of NBT photoreduction.

Enzymes related to N metabolism were assayed according to Borlotti et al. (2012). The nitrate reductase (NR, EC 1.7.1.1) activity was determined by using the colorimetric assay of nitrite performed according to Long and Oaks (1990). The glutamine synthase (GS, EC 6.3.1.2) activity was performed by monitoring the NADH formation according to Scheible et al. (1997); while the NAD(P)H-dependent glutamine-oxoglutarate aminotransferase (NAD(P)H-GOGAT, EC 1.4.1.14) activity was assayed according to Chen and Cullimore (1988).

2.6. Western blot analysis

Purified peroxisomes isolated from leaf of cucumber plants grown in the presence or the absence of Fe for 7 d, were loaded on a discontinuous sodium dodecyl sulfate (SDS)-polyacrylamide gel, [3.75% (w/v) acrylamide stacking gel, and 10–15% (w/v) acrylamide separating gel] (according to the method of Laemmli, 1970).

Electrophoretic transfer to nitrocellulose membrane filters (Sigma, Milan, Italy) was performed in 48 mM Tris, 39 mM glycine, 0.0375% SDS and 20% (v/v) methanol for 1.5 h at room temperature at 0.8 mA cm−2. After blotting, the membrane was incubated for 1 h in PBS-TB blocking buffer [phosphate-buffered saline, 0.1% Tween-20, 1% BSA, (for monoclonal antibodies)] or TBS-TM blocking buffer [Tris-buffered saline, 0.1% Tween-20, 5% commercial dried skimmed milk, (for

polyclonal antibodies)]. Different antibodies were used, and the dilution ratios were: 1:6000 for a-CAT (Yamaguchi et al., 1984), 1:3000 for a-GOX (Nishimura et al., 1983), 1:3000 for a-PEX14 (Hayashi et al., 2000). All these antibodies were a kind gift from Dr Shoji Mano from the Department of Cell Biology, National Institute for Basic Biology, Okazaki, Japan. The incubation in primary antibody, diluted in blocking buffer, was carried out for 2 h at room temperature. After rinsing with TBS-TM or PBS-TB, nitrocellulose membranes were incubated at room temperature for 2 h with a 1:10000 diluted secondary antibodies [alkaline phosphatase-conjugated anti-rabbit (for polyclonals) or anti-mouse (for monoclonals) [IgG, Sigma, Milan, Italy]. After rinsing in TBS-T (Tris-buffered saline, 0.1% Tween-20) or PBS-T (phosphate-buffered saline, 0.1% Tween-20), filters were incubated in 5-bromo-4-chloro-3-indolyl phosphate and nitroblue tetrazolium (FAST BCIP/NBT, Sigma) for detection.

2.7. Native PAGE and SOD isoform visualization

Superoxide dismutase isoforms extracted from control and Fe-deficient plants 7 d after the start of the treatment as reported above, were separated by 12.5% native polyacrylamide gel electrophoresis (PAGE) at 100 V using the method described by Beauchamp and Fridovich (1971). Pre-treatment of the gels with 5 mM H_2O_2 and 3 mM KCN before SOD staining allowed us to characterize SOD isoforms as Cu/Zn-SOD, Fe-SOD or Mn-SOD because the isoenzymes were selectively inhibited by KCN or H_2O_2. In particular, Mn-SOD is resistant to both inhibitors, Fe-SOD is resistant to KCN and inhibited by H_2O_2, and both inhibitors inhibit Cu/Zn-SOD.

2.8. H_2O_2 content evaluation

H_2O_2 content in leaves from control and Fe-deficient plants 7 d after the start of the treatment, was measured following the method reported by Ranieri et al. (2001) based on the formation of the titanium-peroxide complex. The leaf samples were homogenized in cold 100% acetone (1:2; w/v), and centrifuged at 10000 g for 10 min; then 20% $TiCl_4$ in concentrated HCl was added to supernatant aliquots to give a final titanium concentration of 4%. After addition of NH_4OH (0.2 mL for each mL of the sample) to precipitate the titanium-peroxide complex, samples were centrifuged at 10000 g for 5 min, and the resulting pellet was washed five times in acetone and then resuspended in 2 N H_2SO_4. The absorbance of the solution was read at 415 nm against a blank containing H_2O instead of extracts.

2.9. Nitrate and ammonium analysis by capillary electrophoresis

Leaves from control (+Fe) and Fe-deficient (-Fe) plants 7 d after the start of the treatment were harvested 4 h after onset of light and immediately frozen in liquid nitrogen, and the plant material was stored at −80 °C. Nitrate and ammonium were extracted from the leaves with ultrapure water. Extracts were filtered through 0.2 µm filters and then analyzed by an Agilent 7100 Capillary Electrophoresis System (Agilent Technologies, Santa Clara, CA, US). Ammonium was analyzed using a bare fused silica capillary with extended light path BF3 (i.d. = 50 µm, I = 56 cm, L = 64.5 cm). Sample injection was at 50 mbar for 5 s with +30 kV voltage and detection wavelength at 310/20 nm. Nitrate and nitrite were analyzed using a bare fused silica capillary with extended light path BF3 (i.d. = 50 µm, I = 72 cm, L = 80.5 cm). Sample injection was at 50 mbar for 4 s with −30 kV voltage and detection at 350/80 nm wavelength. Compounds were identified by using pure standards. The ion content was expressed as mg g−1 FW.

2.10. Amino acid analysis

Amino acid (AA) analysis was performed on leaves of both Fe-deficient (-Fe) and control (+Fe) plants. Free AA were extracted from fresh tissues at 4 °C, first in 80% ethanol overnight, then in 60% ethanol for 1 h and finally in distilled water for 24 h. The supernatants of each sample were pooled, aliquoted and kept at −20 °C. Free amino acids were determined by HPLC as described before (Muller and Touraine, 1992).

2.11. Miscellaneous

RNA was purified from leaves from control and Fe-deficient plants 7 d after the start of the treatment and harvested 4 h after onset of light, according to Borlotti et al. (2012). Northern blot analysis procedures were carried out according to Borlotti et al. (2012). Gene sequences considered were Csa015274 (CsGS1), Csa0081189 (CsGS2), Csa021126 (CsNADH-GOGAT), Csa002676 (CsFd-GOGAT), Csa008224 (CsNR) according to Borlotti et al. (2012).

Metal contents were determined in dried leaf tissues after mineralization in HNO3 by using a Microwave Digestion System (Multiwave ECO). Inductively coupled plasma-mass spectrometry (ICP/MS, aurora M90 BRUKER) was used to quantify the content of iron (Fe), manganese (Mn), copper (Cu) and zinc (Zn) according to Vigani et al. (2018).

Total protein concentration was determined by using the dye-binding method of Bradford (1976), using BSA as a standard.

Statistical analyses were conducted with Past 3 software. Student's t-test was used to compare the means (three independent experiments ±standard deviation) at the $P \leq 0.05$ level in all cases.

3. Results

3.1. Gas exchange parameters in cucumber leaves under Fe deficiency

After 7 d of Fe deficiency, cucumber leaves had a strong alteration in the CO2 assimilation rate in response to increasing light or intercellular CO2 concentration as evidenced by gas exchange parameters derived by the analysis of light curve and A/Ci response curves (Table 1; Fig. S1). The reduced ability in carbon assimilation displayed by Fe-deficient plants was evident both under low and saturating light conditions (Supplementary Fig. S1).

Table 1. Gas exchange parameters determined in leaves of cucumber plants subjected for 7 days to the absence (-Fe) or the presence of 50 µM Fe (+Fe) in the nutrient solution. Parameters derived from the light curves determined at 21 and 2% pO2 and A/Ci curve. For details see Materials and Methods section. Each value represents the means of three replicates (±standard deviation). In the last column, the significance of the difference between the means following Student's t-test is reported.

21% pO2

Parameters	+Fe	-Fe	p
A390 (µmol CO2 m−2s−1)	10.4 (0.2)	1.7 (0.7)	***
gs (mmol H2O m−2s−1)	233.8 (22.4)	110.5 (3.5)	**
Ci (µmol CO2 mol−1 air)	283.5 (13.1)	367.0 (1.4)	**
Rd (µmol CO2 m−2s−1)	1.6 (0.7)	1.2 (0.2)	ns
ΦCO2 (µmol CO2 µmol photons)	0.05 (0.01)	0.008 (0.004)	**

Vc,max (mmol CO2 m−2s−1)	87 (7.0)	26 (4.1)	***

2% pO2

Parameters	+Fe	-Fe	p
A390 (µmol CO2 m−2s−1)	18.2 (1.5)	2.4 (0.2)	***
gs (mmol H2O m−2s−1)	253.0 (15.6)	158.5 (14.9)	***
Ci (µmol CO2 mol−1 air)	247 (10.0)	354 (0.70)	**
ΦCO2 (µmol CO2 µmol photons)	0.07 (0.01)	0.012 (0.002)	ns

A390: photosynthetic rate at ambient CO2 and light-saturated conditions; gs: stomatal conductance to water vapour at ambient CO2 and light-saturated conditions; Ci: intercellular CO2 concentration at ambient CO2 and light-saturated conditions; Rd: dark respiration at ambient CO2 and in the dark; ΦCO2: quantum yield for CO2 uptake; Vc, max: in vivo carboxylation efficiency of Rubisco enzyme. ***: P < 0.001; **: P < 0.01; ns: P > 0.05.

The quantum yield for CO2 assimilation, ΦCO2, was significantly reduced in Fe-deficient plants, indicating a reduction in the efficiency of the use of CO2 per mole of absorbed photons (Table 1). A substantial reduction in CO2 assimilation was also observed in saturating light conditions (−84% of A390 in comparison with the controls; Table 1). Likewise, as deduced by the gas exchange parameters, the reduction of CO2 assimilation was attributable to a reduced stomatal conductance, but also to an alteration in the activity of the mesophyll considering the increase in the intercellular CO2 concentration (Ci) (Table 1). On the other hand, Vc, max, that indicates the in vivo carboxylation activity of the enzyme ribulose-1,5-bisphosphate carboxylase/oxygenase (Rubisco), was strongly and significantly reduced in Fe-deprived leaves as compared to the controls (−87%).

Chlorophyll a fluorescence analysis (Table 2) underlined the altered photochemical efficiency of PSII (i.e. the significant reduction of Fv/Fm and ΦPSII) in Fe-deprived leaves (Table 2). The photochemical quenching coefficient, qP, and the electron transport rate (ETR) in light conditions sharply decreased in Fe-deprived leaves (−68 and −73% as compared to their controls, respectively) while Fe-deficient leaves exhibited a remarkable increase in NPQ.

Table 2. Chlorophyll fluorescence parameters determined in leaves of cucumber plants subjected for 7 days to the absence of Fe (-Fe) or the presence of 50 µM Fe (+Fe) in the nutrient solution. Each value represents the means of three replicates (±standard deviation). In the last column, the significance of the difference between the means following Student's t-test is reported.

PARAMETERS	+Fe	-Fe	p
F0	196 (12)	330 (24)	***
Fm	993 (114)	550 (38)	***
Fv/Fm	0.81 (<0.01)	0.43 (0.09)	***
ETR (µmol electron m−2 s−1)	110.7 (26.4)	13.5 (1.7)	***
ΦPSII	0.46 (0.05)	0.05 (<0.01)	***
qp	0.53 (0.13)	0.14 (0.03)	***
NPQ	0.41 (0.03)	2.06 (0.12)	***

F0: minimal fluorescence determined in dark conditions; Fm: maximal fluorescence determined in dark conditions; Fv/Fm: potential quantum yield of PSII; ETR: electronic transport rate; ΦPSII:

photochemical PSII efficiency (in light conditions); qP photochemical quenching coefficient; NPQ: non-photochemical quenching. ***: P < 0.001.

3.2. Estimation of photorespiration impairment under Fe deficiency

Modelling of light response curves at both 21 and 2% pO2 in control leaves suggest a slightly higher A390 asymptote at 2% as compared to the same analysis at 21% (pO2) (Fig. S1B). Thus, stimulation of CO2 assimilation rate by low pO2 was expected, considering the elimination of the photorespiration process (Table 1). Even in Fe-deprived leaves, the absence of O2 induced an increase in CO2 assimilation rate.

The obtained results indicate that photorespiration contributes to the decrease of assimilated CO2 by 43% and 29%, in controls and Fe-deprived leaves, respectively (Table 1). Such results suggested that the photorespiration process is still active under Fe deficiency, even though at a low rate.

3.3. Fe deficiency affects the biochemical activity of peroxisomes in leaves

In order to investigate the effect of Fe deficiency on photorespiration, we purified the peroxisome fraction from leaf tissues. The first reaction of photorespiration into peroxisome, i.e. the conversion of glycolate to glyoxylate, is carried out by the (enzyme) glycolate oxidase. During this reaction, H2O2 is typically generated as a by-product and then scavenged by CAT. Therefore, the determination of GOX and CAT activities was performed on the peroxisome purified fraction. As shown in Fig. 1A, Fe deficiency did not significantly affect the GOX activity. Accordingly, Western Blot analysis performed on the peroxisomal purified fraction LP-P1 did not reveal differences in the expression of glycolate oxidase protein under Fe deficiency condition (see Supplementary Material,Supplementary Fig. S2). However, CAT activity decreased by about 35% in the leaves of cucumber plants after 7d of growth under Fe deficiency as compared with the controls (Fig. 1B). Accordingly, the concentration of H2O2 in the leaves was higher (+40%) in the absence of Fe (Fig. 2A). Such H2O2 accumulation might be linked to the metal imbalance observed in Fe-deficient leaves (Fig. 2B) as well as to a different modulation of SOD activities (Fig. 2C). Fe-deficient leaf displayed a decrease of Fe (−60%) content along with an accumulation of Zn (+155%) and Cu (+55%) respect to the control (Fig. 2B). Accordingly, the in gel-activity of the Cu/Zn-SOD isoforms is higher as compared with the controls, whereas in the same leaves the activity of Fe-SOD was lower compared with the control condition (Fig. 2C). Although Mn content did not change, Mn-SOD in gel activity decreased in Fe-deficient leaves.

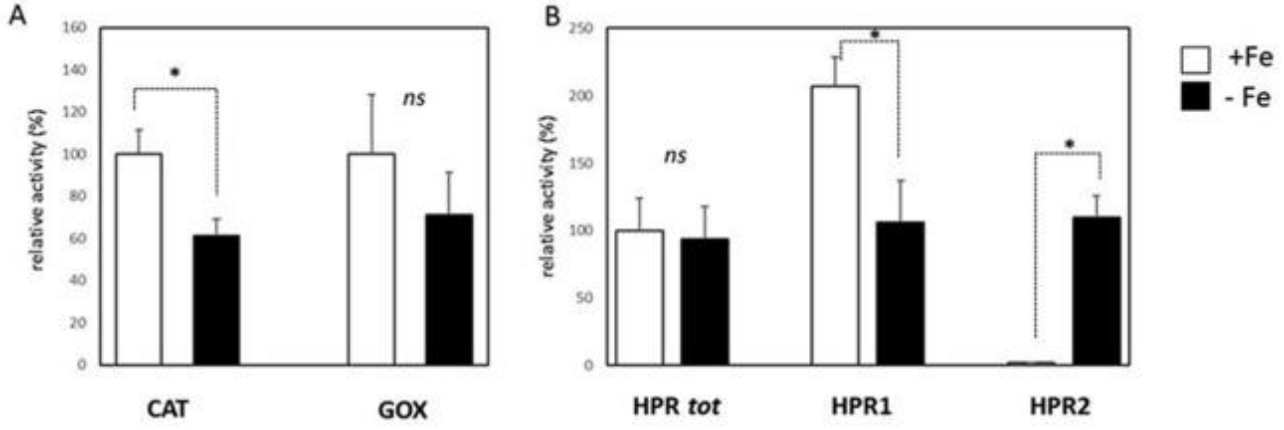

Fig. 1
Download : Download high-res image (134KB)Download : Download full-size image
Fig. 1. Enzymatic activity of catalase (CAT), glycolate oxidase (GOX), total hydroxypyruvate reductase (HPR), HPR cytosolic (HPR2) and peroxisomal (HPR1) isoforms in leaves of cucumber plants grown in the presence (50 mM FeEDTA; white bar) or absence of Fe (black bar) for 7 days. Data are the means of three independent experiments (±standard deviation). The activities are expressed as percentage (%) of the relative activity of the Fe-deficient samples compared to control (+Fe) plants. Activity of control (+Fe) was 132.47, 12.23, 11.78 nmol NADH mg−1 prot min−1, for CAT, GOX and HPR (total activity) respectively. The asterisks indicate the significance following the Student's t-test for the comparison between -Fe and + Fe leaves. ns: $P > 0.05$; *$P < 0.05$.

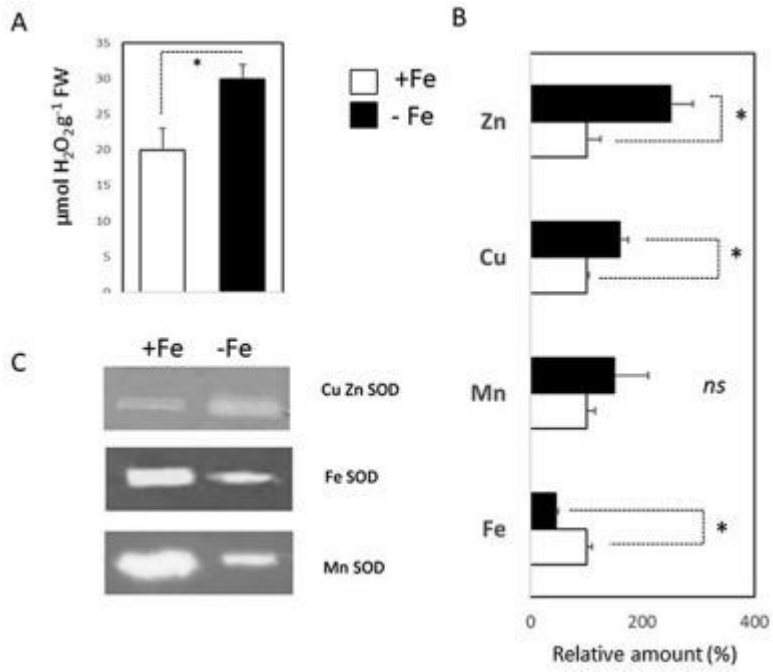

Fig. 2
Download : Download high-res image (142KB)Download : Download full-size image
Fig. 2. Concentration of hydrogen peroxide (A); in-gel SOD isoforms activities assay (B), and metal content (Fe, Mn, Cu and Zn; C) in leaves of cucumber plants grown in the presence (50 mM FeEDTA; white bar) or absence of Fe (black bar) for 7 days. Metal contents are expressed as relative amount (%) of –Fe respect to + Fe leaf samples. The content of metals in +Fe was 148.32, 28.45, 18.97, 34.21 µg g−1 DW for Fe, Mn, Cu and Zn respectively. Discrimination among isoforms was performed using KCN, H2O2 or both as inhibitors (see Materials and Methods); 12 µg protein per lane. Data are the mean (or the representative gel) of three independent experiments (±standard deviation). In Fig. 2A, the asterisks indicate the significance following the Student's t-test for the comparison between -Fe and + Fe leaves. ns: $P > 0.05$.

The lack of Fe during the plant growth did not affect the total HPR activity in the leaves of cucumber plants (Fig. 1B). Interestingly, by discriminating the activity of the two HPRs isoforms (cytosolic, HPR2 and peroxisomal, HPR1), in control leaves the total HPR activity was entirely attributable to the peroxisomal isoform (HPR1), while a very low cytosolic isoform (HPR2) activity was observed. On the contrary, in plants grown in Fe-deficient condition, the two isoforms of HPR had a similar activity (Fig. 1B), significantly lower than in the controls in peroxisome but significantly higher in

cytosol as compared with the controls. Finally, the activity of G3PDH was sharply increased in leaves of plants subjected to Fe deficiency (Supplementary Fig. S4).

3.4. Fe deficiency affects nitrogen (N) metabolism in cucumber leaves

An imbalance in the N metabolism was observed in plants subjected to Fe deficiency (Fig. 3). Although under Fe deficiency NR activity strongly decreased, GS activity was not affected, and the GOGAT (NADPH-dependent isoform) activity was induced (Fig. 3A). The expression of the relative genes partially mirrored what was observed at enzymatic level: under Fe deficiency the expression of CsNR gene decreased, while the expression of genes encoding for the GS isoforms was not affected (CsGS1) or induced (CsGS2). Furthermore, the expression of genes encoding for GOGAT isoforms did not change in Fe-deficient leaves compared with control plants (Supplementary Fig. S3). The alteration of nitrate reduction and ammonium organisation process led to the increase of NO3− content, as well as to unchanged level of NH4+ in Fe-deficient leaves with respect to control plants (Fig. 3B). Furthermore, the concentration of the amino acids in leaves changed under Fe deficiency conditions (Table 3). The content of arginine (Arg), asparagine (Asn) glutamine (Gln), and serine (Ser) accumulated in Fe-deficient leaves, while aspartate (Asp) and glutamate (Glu) did not change in their content in Fe-deficient leaves as compared to controls (Table 3). Besides, glycine (Gly) content decreased in Fe-deficient leaves (Table 3).

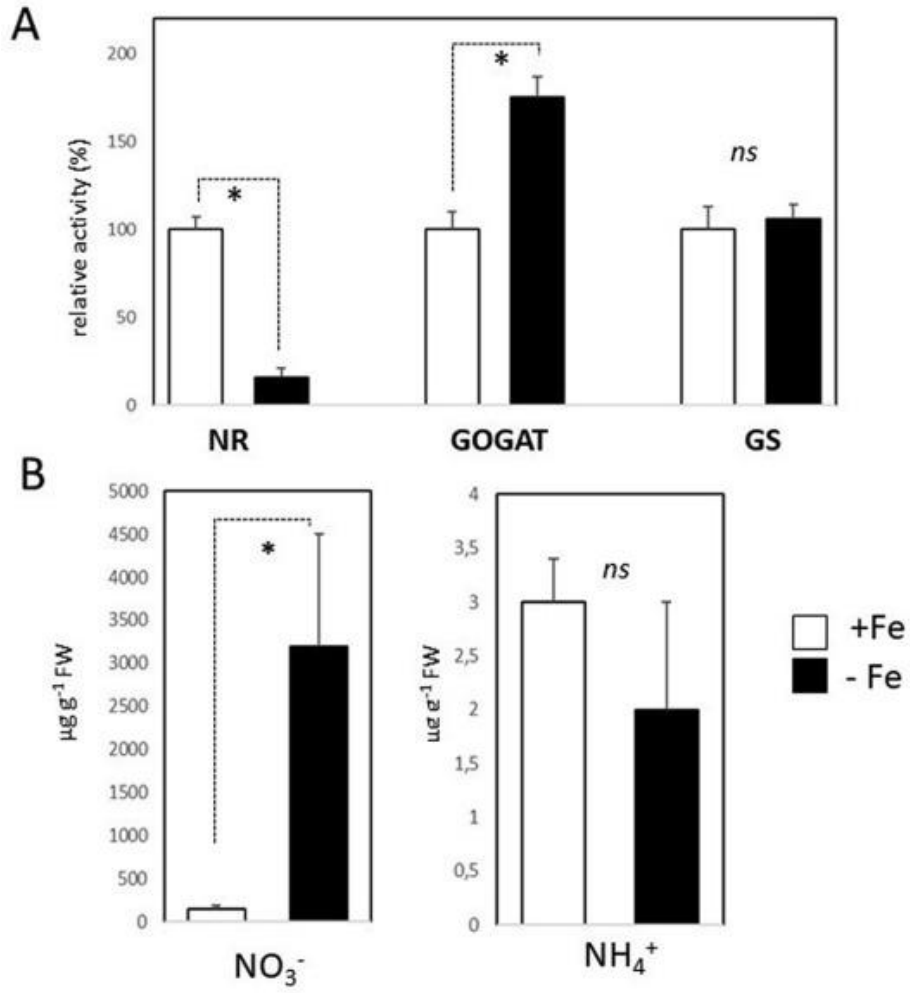

Fig. 3

Download : Download high-res image (271KB)Download : Download full-size image

Fig. 3. N assimilation-related enzyme and nitrate and ammonium content in leaves of cucumber plants grown in the presence (+Fe, 50 mM FeEDTA; white bar) or absence (-Fe) of Fe (black bar) for 7 days. (A) Enzymatic activity of nitrate reductase (NR), glutamine oxoglutarate aminotransferase (GOGAT) glutamine synthase (GS). The activities are expressed as percentage (%) of the relative activity of the Fe-deficient samples compared to control (+Fe) plants. Activity of control (+Fe) was 11.21, 132.45, 225.67 nmol NADH mg−1 prot min−1, respectively for NR, GOGAT and GS, respectively. (B) Nitrate (NO_3^-) and ammonium (NH_4^+) content in leaves. Data are expressed as µg g−1 FW. Data are the means of three independent experiments (±standard deviation). The asterisks indicate the significance following the Student's t-test for the comparison between -Fe and + Fe leaves. ns: $P > 0.05$; *: $P < 0.05$.

Table 3. Amino acid concentration (expressed as nmol mg−1 FW) in leaves of cucumber plants subjected for 7 days to the absence of Fe (-Fe) or the presence of 50 µM Fe (+Fe) in the nutrient solution. Each value represents the means of three independent experiments (±standard deviation). In the last row, the significance of the difference between the means following Student's t-test is reported.

Treatment	Asp	Glu	Asn	Ser	Gln	Gly	Arg
+Fe	0.88 (0.053)	2.65 (0.395)	0.08 (0.013)	0.29 (0.044)	0.44 (0.030)	0.13 (0.031)	0.15 (0.048)
-Fe	0.87 (0.156)	2.90 (1.710)	0.17 (0.058)	0.49 (0.258)	0.87 (0.615)	0.05 (0.035)	0.40 (0,099
P	ns	ns	*	*	*	*	*

ASP: aspartic acid; GLU: glutamic acid; ASN: asparagine; SER: serine; GLN: glutamine; GLY: glycine; ARG: arginine. ns: $P > 0.05$; *: $P < 0.05$.

4. Discussion

It is well known that under Fe deficiency, leaves generally display low photosynthetic activity (Abadía et al., 1999; Hantzis et al., 2018), enhancing the risk for photo-oxidative damage, especially to PSII (Andersson and Aro, 2001).

Data obtained in this work confirm that Fe deficiency strongly impaired the photosynthetic machinery at different levels. The substantial decrease in CO_2 assimilation can be related to several changes occurring in Fe-deficient leaves: i) stomatal closure; ii) biochemical reduction of CO_2 assimilation, as evidenced by the decrease in carboxylation activity of Rubisco enzyme, iii) decrease in PSII photochemical efficiency (i.e. the reduction in Fv/Fm and ΦPSII) and a sharp decrease of ETR. The decrease in Fv/Fm, observed in Fe-deficient leaves, is attributable to the increase in the minimal as well as to the decrease in maximal chlorophyll fluorescence. An increases in F0 [which represents the minimal fluorescence yield and occurs when all reaction centres are in an open state (Krause and Weiss, 1991)] under Fe deficiency might indicate losses of energy transfer from pigments to the reaction center, likely due to damage of the LHC associated with the PSII, as previously observed in conditions of Fe deficiency (Abadía et al., 1999). However, the analogous decrease of Fm yield reflects the increase of energy dissipation which may be related to denaturation of chlorophyll-binding proteins (Yamane et al., 1998), such as the antenna pigment-protein complex CP43-CP47 (Wang et al., 1999) and/or irreversible photo-damage to the RCII (Klughammer and Schreiber,

2008). However, NPQ increased in Fe-deficient leaves of cucumber plants, which is supportive for the activation of photo-protective mechanisms by these plants. These findings are in agreement with the previous investigations performed in other species, such as in pear (Morales et al., 2000a, b), tomato (Donnini et al., 2003), peach (Molassiotis et al., 2006), and pea (Jelali et al., 2011). Hantzis et al. (2018) reported that Fe-deficient Arabidopsis plants displayed lower values of NPQ as compared with control plants, suggesting that some plants displayed different modulation of photosynthetic process under low Fe availability. Later authors also demonstrated that a hierarchy for Fe utilization in photosynthetic tissue occurs in plants, indicating that different plant species/genotypes might display specific Fe-economy programs and, in turn, different acclimation strategies to avoid Fe deficiency (Vigani and Murgia, 2018).

In addition to photosynthetic-related parameters, this work offers new insights on the impact of Fe deficiency on the PR pathway. The amount of CO2 assimilated is less affected by PR under Fe deficiency compared with control plants, indicating that such a pathway is slowed down when hardly any Fe is present. Accordingly, the in vivo carboxylation activity is strongly impaired while GOX activity did not change and CAT activities decreased under Fe deficiency. Such observations suggest that the modulation of both photosynthesis and photorespiration under low Fe availability allows plants to limit the losses of CO2 assimilation by PR.

Along with CO2 assimilation, the metabolic pathway of PR is interlinked to the N metabolism. The presence of the so-called photorespiratory N cycle allows the reincorporation of NH4+, coming from Gly-Ser conversion, into Glu/Gln via GS-GOGAT cycle (Keys et al., 1978). Thanks to the ability of GOGAT to provide Glu also to Glutamate:Glyoxylate aminotransferase (GGAT) in the peroxisome, the NH4+ recycled can be used for the synthesis of new Gly molecules. In this work, Fe deficiency affected peroxisome metabolism as well as photorespiratory N recycling by altering NO3− reduction, ammonia organication, and quali-quantitative amino acid composition in leaves. Such observations agree with the finding that under Fe deficiency, NR activity sharply decreased in leaves leading to foliar NO3− accumulation. On the other hand, the GS-GOGAT cycle was not impaired, and NH4+ content did not show any changes under Fe deficiency, to indicate that NH4+ content derived from AA recycling instead of from NO3− reduction. Furthermore, under Fe deficiency, the Gly content decreased in cucumber leaf along with an accumulation of Ser. Such findings suggest that the conversion of Gly into Ser is maintained at high rate under Fe deficiency. Such a reaction represents a crucial step to produce NH4+ for photorespiratory N cycling (Peterhansel and Maurino, 2011). However, in addition to PR, two other pathways of Ser formation operate in plants and represent the branches of glycolysis diverging at the level of 3-phosphoglyceric acid. One branch (the glycerate–serine pathway) occurs in the cytosol and involves glycerate formation from 3-phosphoglycerate, while the other (the phosphorylated serine pathway) operates in plastids and forms phosphohydroxypyruvate as an intermediate (Igamberdiev and Kleczkowski, 2018). The differential modulation of hydroxypyruvate reductase (HPR) 1 and HPR2 activities occurred under Fe deficiency, which suggests that Ser synthesis from the non-phosphorylated pathways is unlikely to be induced under Fe deficiency. Hydroxypyruvate (Hpyr) can diffuse out of the peroxisome to the cytosol, where it is converted into glycerate by HPR2, a cytosolic paralog of peroxisomal HPR1 (Timm et al., 2008, Timm et al., 2012). Recent work reported that Hpyr in the cytosol might be involved in the alternative PR pathway involving glycerate kinase (GLYK) (Ushijima et al., 2017). This enzyme catalyzes the conversion of glycerate to 3-phosphoglycerate (3PGA) during the final step of photorespiration in the chloroplast (Boldt et al., 2005; Peterhansel and Maurino, 2011). However, a

cytosolic isoform of GLYK has recently been identified in the plant, which catalyzes the conversion of the cytosolic glycerate into 3PGA (Ushijima et al., 2017). The level of Gly, a photorespiratory intermediate, accumulated at significantly lower levels in GLYK overexpressing mutant (cytGLYK) plants than in the glyk mutant (Ushijima et al., 2017). Such findings may indicate that the low level of Gly observed in Fe-deficient leaves might be linked to the higher induction of the cytosolic photorespiratory pathway through the activation of HPR2. Therefore, the observed compensation HPR activity between peroxisomal and cytosolic isoforms along with the induction of G3PDH cytosolic activity suggest that Hpyr synthesized in the peroxisome is probably addressed to glycolysis throughout the cytosolic photorespiratory bypass (Fig. 4) (Ushijima et al., 2017).

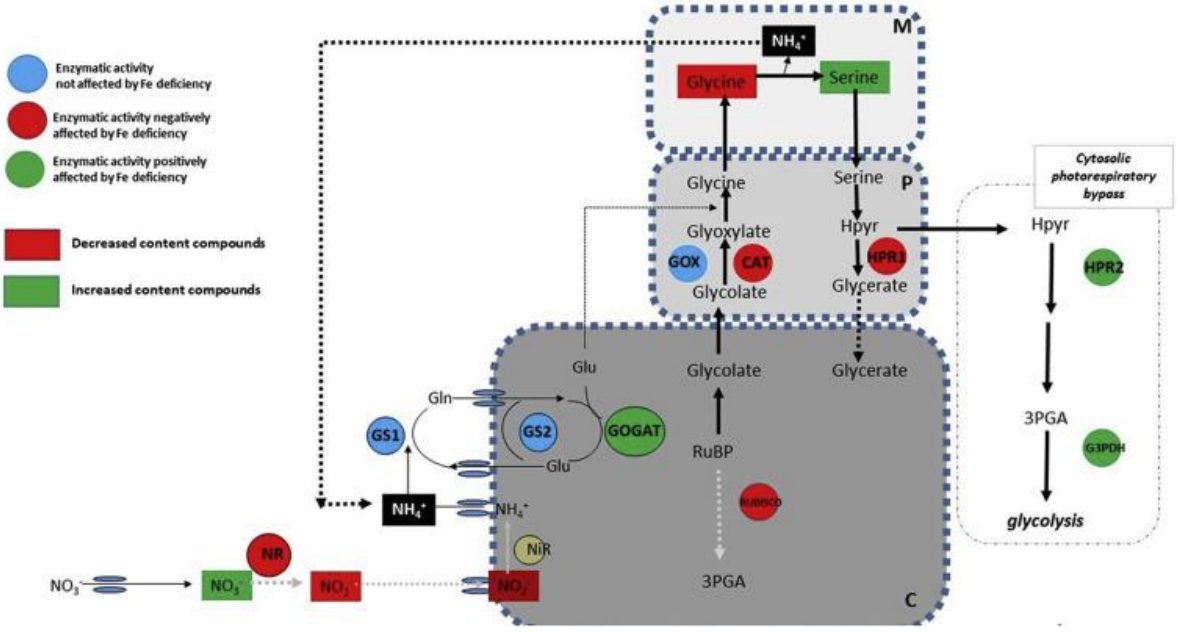

Fig. 4

Download : Download high-res image (518KB)Download : Download full-size image

Fig. 4. Schematic representation of photorespiratory modulation and N recycling in Fe-deficient cucumber leaves. Fe deficiency determines i) a decrease (red circle) and an increase (green circle) of some enzymatic activities and ii) the accumulation (green rectangle) and a decreased content (red rectangle) of some compounds related to photorespiratory and N assimilation pathways. Proposed metabolic changes allow us to hypothesize that Fe deficiency leads to metabolic alterations aimed at sustaining N recycling and cytosolic photorespiratory bypass.

AbbreviationsC, chloroplast; P, peroxisome; M, mitochondrion; NR, nitrate reductase: GOGAT, glutamine oxoglutarate aminotransferase; glutamine synthase (GS); HPR, hydropyruvate reductase; Hpyr; PGA and 3PGA. (For interpretation of the references to color in this figure legend, the reader is referred to the Web version of this article.)

Overall, this work provides substantial evidence about the modulation of the PR in cucumber leaves under Fe deficiency. Our results suggest that plants subjected to Fe deficiency modulate PR-related processes, i.e. activating N recycling and cytosolic photorespiratory bypass, to sustain ammonia organication and glycolysis pathway respectively. A role of PR in the metabolic reprogramming occurring under Fe deficiency in cucumber leaves was highlighted, which adds a new piece to the puzzle of Fe metabolism in plants.

Contributions

GV, GZ and LG conceived the experimental work; FMC, ML, SD, LG performed the experimental analysis. GV drafted the manuscript, ML, LG, GZ revised critically the manuscript.

CRediT authorship contribution statement

Fabio M. Casiraghi: Investigation, Methodology, Formal analysis. Marco Landi: Investigation, Formal analysis, Writing - review & editing. Silvia Donnini: Investigation, Formal analysis. Andrea Borlotti: Investigation, Formal analysis. Graziano Zocchi: Writing - review & editing. Lucia Guidi: Methodology, Validation, Writing - review & editing. Gianpiero Vigani: Conceptualization, Resources, Writing - original draft, Writing - review & editing.

Declaration of competing interest

The authors declare that the research was conducted in the absence of any commercial or financial relationships that could be construed as a potential conflict of interest.

Acknowledgements

Research was supported by the local research funds of the Department of Life Science and Systems Biology, University of Turin.

Appendix A. Supplementary data

The following are the Supplementary data to this article:

Supplementary Fig. S1

Download : Download high-res image (169KB)Download : Download full-size image

Supplementary Fig. S1. Response curve of CO2 assimilation in relation to intercellular CO2 concentration (A/Ci curves) in leaves of cucumber control (round) and Fe deficient plants (square) after 7 days from the start of the experiment (A). A/Ci curves were determined at saturating light intensity, and each value represents the mean of three replicates. The response curve of the photosynthetic activity to increasing light intensity (light curves) under conditions of 21% O2 (round symbol) and in the absence of O2 (square symbol). Light curves were determined at 380 µmol mol−1 CO2, and each value represents the mean of three replicates.

Supplementary Fig. S2

Download : Download high-res image (71KB)Download : Download full-size image

Supplementary Fig. S2. A) Western blot analysis of the different fraction of the mixed Percoll-Sucrose gradient on leaves of control plants (+Fe) and Fe deficient plants (-Fe). For each sample, 10 µg of protein was used. Antibody used was against catalase. CAT catalase; CE crude extract: S1 supernatant 1; I Percoll-Sucrose interface; B bottom of the centrifugation tubes. B) Western blot analysis of in leaves of control plants (+Fe) and Fe deficient plants (-Fe) after 7 days from the start of the experiment. For each sample, 12 µg of protein was used. Antibody used was against Glycolate oxidase. GOX catalase; LP-P1 Leaf peroxisome purified fraction

Supplementary Fig. S3

Download : Download high-res image (94KB)Download : Download full-size image

Supplementary Fig. S3. Northern blot analysis of genes involved in N assimilation pathway in leaves of cumber control (+Fe) and Fe deficient plants (-Fe)after 7 days from the start of the experiment.

Gene sequences considered were Csa015274 (CsGS1), Csa0081189 (CsGS2), Csa021126 (CsNADH-GOGAT), Csa002676 (CsFd-GOGAT), Csa008224 (CsNR) according to Borlotti et al. (2012).

Supplementary Fig. S4
Download : Download high-res image (117KB)Download : Download full-size image
Supplementary Fig. S4. Activity of glyceraldehyde 3 phosphate dehydrogenase in leaves of cucumber control (+Fe) and Fe deficient plants (-Fe). The asterisks indicate the significance following the Student's t-test for the comparison between -Fe and + Fe leaves. ns: $P > 0.05$; *$P < 0.05$.

References

Abadía et al., 1999
J. Abadía, F. Morales, A. Abadía
Photosystem II efficiency in low chlorophyll, iron-deficient leaves
Plant Soil, 215 (1999), pp. 183-192, 10.1023/A:1004451728237
View Record in ScopusGoogle Scholar
Andersson and Aro, 2001
B. Andersson, E.M. Aro
Photodamage and D1 protein turnover in photosystem II
E.M. Aro, B. Andersson (Eds.), Regulation of Photosysthesis, Kluwer Academic Publisher, Dordrecht, The Netherlands (2001), pp. 377-393
View Record in ScopusGoogle Scholar
Araújo et al., 2012
W.L. Araújo, T. Tohge, A. Nunes-Nesi, D.M. Daloso, M. Nimick, I. Krahnert, V.I. Bunik, G.B.G. Moorhead, A.R. Fernie
Phosphonate analogs of 2-oxoglutarate perturb metabolism and gene expression in illuminated Arabidopsis leaves
Front. Plant Sci., 3 (2012), p. 114, 10.3389/fpls.2012.00114
Google Scholar
Beauchamp and Fridovich, 1971
C. Beauchamp, I. Fridovich
Superoxide dismutase: improved assays and an assay applicable to acrylamide gels
Anal. Biochem., 44 (1971), pp. 276-287, 10.1016/0003-2697(71)90370-8
ArticleDownload PDFView Record in ScopusGoogle Scholar
Belkhodja et al., 1998
R. Belkhodja, F. Morales, R. Quilez, A.F. Lopez-Millan, A. Abadia, J. Abadia
Iron deficiency causes changes in chlorophyll fluorescence due to the reduction in the dark of the Photosystem II acceptor side
Photosynth. Res., 56 (1998), pp. 265-276, 10.1023/A:1006039917599
View Record in ScopusGoogle Scholar
Bilger, 1990
Bilger, Björkman
Role of the xanthophyll cycle in photoprotection elucidated by measurements of light-induced absorbance changes, fluorescence and photosynthesis in leaves of Hedera canariensis
Photosynth. Res., 25 (1990), pp. 175-186, 10.1007/BF00033159
Google Scholar

Borlotti et al., 2012
Borlotti A, G Vigani, G Zocchi, et al.
Iron deficiency affects nitrogen metabolism in cucumber (Cucumis sativus L.) plants
BMC Plant Biol., 12 (2012), p. 189
http://www.biomedcentral.com/1471-2229/12/189
CrossRefGoogle Scholar
Bradford, 1976
M.M. Bradford
A rapid and sensitive method for the quantization of micrograms quantities of protein utilizing the principle of protein-dye binding
Anal. Biochem., 72 (1976), pp. 248-254, 10.1006/abio.1976.9999
ArticleDownload PDFView Record in ScopusGoogle Scholar
Briat and Lobreaux, 1997
J.F. Briat, S. Lobreaux
Iron transport and storage in plants
Trends Plant Sci., 2 (1997), pp. 187-193, 10.1016/S1360-1385(97)85225-9
ArticleDownload PDFView Record in ScopusGoogle Scholar
Chen and Cullimore, 1988
F.L. Chen, J.V. Cullimore
Two Isoenzymes of NADH-dependent glutamate synthase in root nodules of Phaseolus vulgaris L: purification, properties and activity changes during nodule development
Plant Physiol., 88 (1988), pp. 1411-1417, 10.1104/pp.88.4.1411
CrossRefView Record in ScopusGoogle Scholar
Curie and Briat, 2003
C. Curie, J.F. Briat
Iron transport and signaling in plant
Annu. Rev. Plant Biol., 54 (2003), pp. 183-206, 10.1146/annurev.arplant.54.031902.135018
View Record in ScopusGoogle Scholar
Donnini et al., 2003
S. Donnini, A. Castagna, L. Guidi, G. Zocchi, A. Ranieri
Leaf responses to reduced iron availability in two tomato genotypes: T3238FER (iron efficient) and T3238fer (iron inefficient)
J. Plant Nutr., 26 (2003), pp. 2137-2148, 10.1081/PLN-120024270
View Record in ScopusGoogle Scholar
Fanquhar et al., 1980
G.D. Fanquhar, S. von Caemmerer, J.A. Berry
A biochemical model of photosynthetic CO2 assimilation in leaves of C3 species
Planta, 149 (1980), pp. 78-90, 10.1007/BF00386231
Google Scholar
Fernie et al., 2013
A.R. Fernie, H. Bauwe, M. Eisenhut, A. Florian, D.T. Hanson, M. Hagemann, O. Keech, M. Mielewczik, Z. Nikoloski, C. Peterhamsel, S. Roje, R. Sage, S. Timm, S. von Cammerer, A.P.M. Weber, P. Westhoff
Perspectives on plant photorespiratory metabolism
Plant Biol. Stutt, 15 (2013), pp. 748-753, 10.1111/j.1438-8677.2012.00693.x
CrossRefView Record in ScopusGoogle Scholar
Genty et al., 1989

B. Genty, J.M. Briantais, N.R. Baker
The relationship between the quantum yield of photosynthetic electron transport and quenching of chlorophyll fluorescence
Biochem. Biophys. Acta (BBA), 990 (1989), pp. 87-92, 10.1016/S0304-4165(89)80016-9
ArticleDownload PDFView Record in ScopusGoogle Scholar
Guidi et al., 2017
L. Guidi, D. Remorini, L. Cotrozzi, T. Giordani, G. Lorenzini, R. Massai, C. Nali, L. Natali, E. Pellegrini, A. Trivellini, A. Vangelisti, P. Vernieri, M. Landi
The harsh life of an urban tree: the effect of a single pulse of ozone in salt-stressed Quercus ilex saplings
Tree Physiol., 37 (2017), pp. 246-260, 10.1093/treephys/tpw103
View Record in ScopusGoogle Scholar
Hantzis et al., 2018
L.J. Hantzis, G.E. Kroh, C.E. Jahn, M. Cantrellm, G. Peers, M. Pilon, K. Ravert
A program for iron economy during deficiency targets specific Fe proteins
Plant Physiol., 176 (2018), p. 610, 10.1104/pp.17.0149
5 96
Google Scholar
Hasunuma et al., 2010
T. Hasunuma, K. Harada, S.-I. Miyazawa, A. Kondo, E. Fukusaki, C. Miyake
Metabolic turnover analysis by a combination of in vivo 13C-labelling from 13CO2 and metabolic profiling with CE-MS/MS reveals rate-limiting steps of the C3 photosynthetic pathway in Nicotiana tabacum leaf
J. Exp. Bot., 61 (2010), pp. 1041-1051, 10.1093/jxb/erp374
CrossRefView Record in ScopusGoogle Scholar
Hayashi et al., 2000
M. Hayashi, K. Nito, K. Toriyama-Kato, M. Kondo, T. Tamaya, M. Nishimura
AtPex14p maintains peroxisomal functions by determining protein targeting to three kinds of plant peroxisomes
EMBO J., 19 (2000), pp. 5701-5710, 10.1093/emboj/19.21.5701
View Record in ScopusGoogle Scholar
Igamberdiev and Kleczkowski, 2018
A.U. Igamberdiev, L.A. Kleczkowski
The glycerate and phosphorylated pathways of serine synthesis in plants: the branches of plant glycolysis linking carbon and nitrogen metabolism
Front. Plant Sci., 9 (2018), p. 318, 10.3389/fpls.2018.00318
Google Scholar
Jelali et al., 2011
N. Jelali, I.B. Salah, W. M'sehli, S. Donnini, G. Zocchi, M. Gharsalli
Comparison of three pea cultivars (Pisum sativum) regarding their responses to direct and bicarbonate- induced iron deficiency
Sci. Hort., 129 (2011), pp. 548-553, 10.1016/j.scienta.2011.06.010
ArticleDownload PDFView Record in ScopusGoogle Scholar
Kato et al., 2003
M.C. Kato, K. Hikosaka, N. Hirotsu, A. Makino, T. Hirose

The excess light energy that is neither utilized in photosynthesis nor dissipated by photoprotective mechanisms determines the rate of photoinactivation in photosystem II
Plant Cell Physiol., 44 (2003), pp. 318-325, 10.1093/pcp/pcg045
View Record in ScopusGoogle Scholar
Keys et al., 1978
A.J. Keys, I.F. Bird, M.J. Cornelius, P.J. Lea, R.M. Wallsgrove, B.J. Miflin
Photorespiratory nitrogen cycle
Nature, 275 (1978), pp. 741-743, 10.1038/275741a0
1978
CrossRefView Record in ScopusGoogle Scholar
Klughammer and Schreiber, 2008
C. Klughammer, U. Schreiber
Saturation pulse method for assessment of energy conversion in PS I
PAM Appl. Note, 1 (2008), pp. 11-14
View Record in ScopusGoogle Scholar
Krause and Weiss, 1991
G.H. Krause, E. Weiss
Chlorophyll fluorescence and photosynthesis: the basics
Annu. Rev. Plant Physiol. Plant Mol. Biol., 42 (1991), pp. 313-349, 10.1146/annurev.pp.42.060191.001525
CrossRefView Record in ScopusGoogle Scholar
Laemmli, 1970
U.K. Laemmli
Cleavage of structural proteins during the assembly of the head of bacteriophage T4
Nature, 227 (1970), pp. 680-685, 10.1038/227680a0
CrossRefView Record in ScopusGoogle Scholar
Li et al., 2019
J. Li, S. Tietz, J.A. Cruz, D.D. Strand, Y. Xu, J. Chen, D.M. Kramer, J. Hu
Photometric screens identified Arabidopsis peroxisome proteins that impact photosynthesis under dynamic light conditions
Plant J., 97 (2019), pp. 460-474, 10.1111/tpj.14134
View Record in ScopusGoogle Scholar
Li et al., 2019
J. Li, M.S. Weraduwage, A.L. Preiser, S. Tietz, S.E. Weise, D.D. Strand, J.E. Froehlich, D.M. Kramer, J. Hu, T.D. Sharkeya
A cytosolic bypass and G6P shunt in plants lacking peroxisomal hydroxypyruvate reductase
Plant Physiol., 180 (2019), pp. 783-792, 10.1104/pp.19.00256
CrossRefView Record in ScopusGoogle Scholar
Long and Oaks, 1990
D.M. Long, A. Oaks
Stabilization of nitrate reductase in maize roots by chymostatin
Plant Physiol., 93 (3) (1990), pp. 846-850, 10.1104/pp.93.3.846
CrossRefView Record in ScopusGoogle Scholar
Luck, 1965
H. Luck
Catalase

H.U. Bergmeyer (Ed.), Method of Enzymatic Analysis, Academic Press, New York and London (1965), pp. 885-894, 10.1016/B978-0-12-395630-9.50158-4
ArticleDownload PDFView Record in ScopusGoogle Scholar
Macheroux et al., 1991
P. Macheroux, V. Massey, D.J. Thiele, M. Volokita
Expression of spinach glycolate oxidase in Saccharomyces cerevisiae: purification and characterization
Biochemistry, 30 (18) (1991), pp. 4612-4619, 10.1021/bi00232a036
CrossRefView Record in ScopusGoogle Scholar
Molassiotis et al., 2006
A. Molassiotis, G. Tanou, G. Diamantidis, A. Patakas, I. Therios
Effects of 4-month Fe deficiency exposure on Fe reduction mechanism, photosynthetic gas exchange, chlorophyll fluorescence and antioxidant defence in two peach roostocks differing in Fe deficiency tolerance
J. Plant Physiol., 163 (2006), pp. 176-185, 10.1016/j.jplph.2004.11.016
ArticleDownload PDFView Record in ScopusGoogle Scholar
Morales et al., 2000a
F. Morales, R. Belkhodja, A. Abadia, J. Abadia
Energy dissipation in the leaves of Fe-deficient pear trees grown in the field
J. Plant Nutr., 23 (2000), pp. 1709-1716, 10.1080/01904160009382135
CrossRefView Record in ScopusGoogle Scholar
Morales et al., 2000b
F. Morales, R. Belkhodja, A. Abadia, J. Abadia
Photosystem II efficiency and mechanisms of energy dissipation in iron deficient, field grown pear trees (Pyrus communis L.)
Photosynth. Res., 63 (2000), pp. 9-21, 10.1023/A:1006389915424
View Record in ScopusGoogle Scholar
Muller and Touraine, 1992
B. Muller, B. Touraine
Inhibition of NO3 uptake by various phloem translocated amino acids in soybean seedlings
J. Exp. Bot., 43 (1992), pp. 617-623, 10.1093/jxb/43.5.617
CrossRefView Record in ScopusGoogle Scholar
Nishimura et al., 1983
M. Nishimura, Y.D. Akhmedov, K. Strzalka, T. Akazawa
Purification and characterization of glycolate oxidase from pumpkin cotyledons
Arch. Biochem. Biophys., 222 (1983), pp. 397-402, 10.1016/0003-9861(83)90536-2
ArticleDownload PDFView Record in ScopusGoogle Scholar
Peterhansel and Maurino, 2011
C. Peterhansel, V.G. Maurino
Photorespiration redesigned
Plant Physiol., 155 (2011), pp. 49-55, 10.1104/pp.110.165019
CrossRefGoogle Scholar
Ranieri et al., 2001
A. Ranieri, A. Castagna, B. Baldan, G.F. Soldatini
Iron deficiency differently affects peroxidase isoforms in sunflower
J. Exp. Bot., 52 (2001), pp. 25-35, 10.1093/jexbot/52.354.25

View Record in ScopusGoogle Scholar
Reumann and Singhal, 2014
S. Reumann, R. Singhal
Isolation of leaf peroxisomes from Arabidopsis for organelle proteome analysis
J.V. Jorrin-Novo, et al. (Eds.), Plant Proteomics: Methods and Protocols, Methods in Molecular Biology (2014), p. 1072, 10.1007/978-1-62703-631-3_36
Google Scholar
Reumann et al., 2007
S. Reumann, L. Babujee, C. Ma, S. Wienkoop, T. Siemsen, G.E. Antonicelli, N. Rasche, F. Luder, W. Weckwerth, O. Jahn
Proteome analysis of Arabidopsis leaf peroxisomes reveals novel targeting peptides, metabolic pathways, and defense mechanisms
Plant Cell, 19 (2007), pp. 3170-3193, 10.1105/tpc.107.050989
CrossRefView Record in ScopusGoogle Scholar
Reumann et al., 2009
S. Reumann, S. Quan, K. Aung, P. Yang, K. Manandhar-Shrestha, D. Holbrook, N. Linka, R. Switzenberg, C.G. Wilkerson, A.P.M. Weber, L.J. Olsen, J. Hu
In-depth proteome analysis of Arabidopsis leaf peroxisomes combined with in vivo subcellular targeting verification indicates novel metabolic and regulatory functions of peroxisomes
Plant Physiol., 150 (2009), pp. 125-143, 10.1104/pp.109.137703
CrossRefView Record in ScopusGoogle Scholar
Scebba et al., 2003
F. Scebba, I. Pucciarelli, G.F. Soldatini, A. Ranieri
O3-induced changes in the antioxidant systems and their relationship to different degrees of susceptibility of two clover species
Plant Sci., 165 (2003), pp. 583-593, 10.1016/S0168-9452(03)00226-7
ArticleDownload PDFView Record in ScopusGoogle Scholar
Scheible et al., 1997
W.R. Scheible, A. Gonzalez-Fontes, M. Lauerer, B. Muller-Rober, M. Caboche, M. Stitt
Nitrate acts as a signal to induce organic acid metabolism and repress starch metabolism in tobacco
Plant Cell, 9 (5) (1997), pp. 783-798, 10.1105/tpc.9.5.783
View Record in ScopusGoogle Scholar
Schreiber et al., 1986
U. Schreiber, U. Schliwa, W. Bilger
Continuous recording of photochemical and non-photochemical chlorophyll fluorescence quenching with a new type of modulation fluorometer
Photosynth. Res., 10 (1986), pp. 51-62, 10.1007/BF00024185
View Record in ScopusGoogle Scholar
Schwitzguebel and Siegenthaler, 1984
J.P. Schwitzguebel, P.A. Siegenthaler
Purification of peroxisome and mitochondrial from spinach leaf by percoll gradient centrifugation
Plant Physiol., 75 (1984), pp. 670-674, 10.1104/pp.75.3.670
CrossRefView Record in ScopusGoogle Scholar
Sunil et al., 2019
B. Sunil, D. Saini, R.B. Bapatla, V. Aswani, A.S. Raghavendra

Photorespiration is complemented by cyclic electron flow and the alternative oxidase pathway to optimize photosynthesis and protect against abiotic stress
Photosynth. Res., 139 (2019), pp. 67-79, 10.1007/s11120-018-0577-x
CrossRefView Record in ScopusGoogle Scholar
Thomine and Vert, 2013
S. Thomine, G. Vert
Iron transport in plants:better be safe than sorry
Curr. Opin. Plant Biol., 16 (2013), pp. 322-327, 10.1016/j.pbi.2013.01.003
ArticleDownload PDFView Record in ScopusGoogle Scholar
Timm et al., 2012
S. Timm, M. Mielewczik, A. Florian, S. Frankenbach, A. Dreissen, N. Hocken, A.R. Fernie, A. Walter, H. Bauwe
High-to-low CO2 acclimation reveals plasticity of the photorespiratory pathway and indicates regulatory links to cellular metabolism of Arabidopsis
PloS One, 7 (2012), Article e42809
CrossRefGoogle Scholar
Timm et al., 2008
S. Timm, A. Nunes-Nesi, T. Pärnik, K. Morgenthal, S. Wienkoop, O. Keerberg, et al.
A cytosolic pathway for the conversion of hydroxypyruvate to glycerate during photorespiration in Arabidopsis
Plant Cell, 20 (2008), pp. 2848-2859, 10.1105/tpc.108.062265
CrossRefView Record in ScopusGoogle Scholar
Ushijima et al., 2017
T. Ushijima, K. Hanada, E. Gotoh, W. Yamori, Y. Kodama, H. Tanaka, M. Kusano, A. Fukushima, M. Tokizawa, Y.Y. Yamamoto, Y. Tada, Y. Suzuki, T. Matsushita
Light controls protein localization through phytochrome-mediated alternative promoter selection
Cell, 30 (2017), pp. 1316-1325, 10.1016/j.cell.2017.10.018
e12
View Record in ScopusGoogle Scholar
Vigani and Murgia, 2018
G. Vigani, I. Murgia
Iron-requiring enzymes in the spotlight of oxygen
Trends Plant Sci., 23 (2018), pp. 874-882, 10.1016/j.tplants.2018.07.005
ArticleDownload PDFView Record in ScopusGoogle Scholar
Vigani et al., 2017
G. Vigani, D. Di Silvestre, A.M. Agresta, S. Donnini, P. Mauri, C. Gehl, et al.
Molybdenum and iron mutually impact their homeostasis in cucumber (Cucumis sativus) plants
New Phytol., 213 (2017), pp. 1222-1241, 10.1111/nph.14214
CrossRefView Record in ScopusGoogle Scholar
Vigani et al., 2018
G. Vigani, S. Bohic, F. Faoro, B. Vekemans, L. Vincze, R. Terzano
Cellular fractionation and nanoscopic x-ray fluorescence imaging analyses reveal changes of zinc distribution in leaf cells of iron-deficient plants
Front. Plant Sci., 9 (2018), p. 1112, 10.3389/fpls.2018.01112
Google Scholar
Vigani et al., 2019

G. Vigani, A. Solti, S.B. Thomine, K. Phillipar
Essential and detrimental-an update on intracellular iron trafficking and homeostasis
Plant Cell Physiol., 60 (2019), pp. 1420-1439, 10.1093/pcp/pcz091
CrossRefView Record in ScopusGoogle Scholar
Voss et al., 2013
I. Voss, B. Sunil, R. Scheibe, A.S. Raghavendra
Emerging concept for the role of photorespiration as an important part of abiotic stress response
Plant Biol., 15 (2013), pp. 713-722, 10.1111/j.1438-8677.2012.00710.x
CrossRefView Record in ScopusGoogle Scholar
Wang et al., 1999
J. Wang, J. Shan, Q. Xu, X. Ruan, Y. Gong, T. Kuang, N. Zhao
Light- and heat-induced denaturation of photosystem II core-antenna complexes CP43 and CP47
J. Photochem. Photobiol., B, 50 (1999), pp. 189-196, 10.1016/S1011-1344(99)00091-3
ArticleDownload PDFView Record in ScopusGoogle Scholar
Wingler et al., 2000
A. Wingler, P.J. Lea, P.W. Quick, R.C. Leegood
Photorespiration: metabolic pathways and their role in stress protection
Phil. Trans. R. Soc. Lond. Biol. Sci., 355 (2000), pp. 1517-1529, 10.1098/rstb.2000.0712
View Record in ScopusGoogle Scholar
Yamaguchi et al., 1984
J. Yamaguchi, M. Nishimura, T. Akazawa
Maturation of catalase precursor proceeds to a different extent in glyoxysomes and leaf peroxisomes of pumpkin cotyledons
Prot. Natl. Acad. Sci USA, 81 (1984), pp. 4809-4813, 10.1073/pnas.81.15.4809
CrossRefView Record in ScopusGoogle Scholar
Yamane et al., 1998
Y. Yamane, Y. Kashino, H. Koike, K. Satoh
Effects of high temperatures on the photosynthetic systems in spinach: oxygen-evolving activities, fluorescence characteristics and the denaturation process
Photosynth. Res., 57 (1998), pp. 51-59, 10.1023/A:1006019102619
View Record in ScopusGoogle Scholar